PAPER

Highly proton conductive and stable sulfonated poly(arylene-alkane) for fuel cells with performance over 2.46 W cm^{-2}†

Wenhao Li,[abc] Run Zhang,[bc] Xiaoyu Zhao,[bc] Zhouying Yue,[b] Huidong Qian ID *[bc] and Hui Yang ID *[ab]

Polyaromatic proton exchange membranes (PEMs) are considered an ideal alternative to perfluorosulfonic acid (PFSA) membranes because of their low-cost and intrinsic low permeability. However, a PEM fuel cell's performance and stability with aromatic PEMs are lower than those with PFSA membranes due to the insufficient proton conductivity and chemical degradation. Herein, we highlight the synthesis of sulfonated poly(arylene-alkane) (Poly(FLx-BPy)-SO$_3$H) PEMs with a comb-like structure design of the combination of rigid ether-free backbones and locally double sulfohexyl flexible side-chains, which would enable high proton conductivity and good chemical stability. Such a comb-like structure leads to the well-developed microphase separation morphology and dense ion clusters or continuous ion channels within the membranes, thus ensuring the highest proton conductivity of 0.115 S cm^{-1} at 25 °C and favorable anti-oxidative stability. Importantly, a H$_2$/O$_2$ PEM fuel cell (PEMFC) using an identical Poly(FL50-BP50)-SO$_3$H membrane and ionomer presents an outstanding power density over 2.46 W cm^{-2} under 2 bar backpressure at 80 °C, which is one of the best-reported results. In the meantime, the PEMFC with this membrane exhibits an excellent stability owing to the ether-free structure and high interfacial compatibility. The comb-like design, ether-free structure and identical membrane and ionomer provide insight into the development of advanced polyaromatic PEMs.

Introduction

Commercially available PFSA membranes such as Nafion membranes have been the benchmark over the last few decades because of their outstanding proton conductivity, mechanical properties, desired oxidative stability, *etc.*[1,2] Nevertheless, the high cost, environmental harm, gas crossover and complex preparation processes prevent their large-scale commercialization.[3] Hence, it has become a new focus to prepare low-cost hydrocarbon-based PEMs. A large number of aromatic polymers, such as poly(arylene ether ketone),[4–6] poly(arylene ether sulfone),[7,8] poly(phenylene),[9] polyimide,[10] poly(benzimidazole)[11–13] and poly(arylene ether)[14] have been prepared as alternatives to PFSA membranes. Nevertheless, there are still few low-cost aromatic PEMs having high-performance and durability comparable to Nafion membranes due to their low ion exchange capacity (IEC), obscure microphase

separation, chemical degradation[15] and incompatibility with PEMs and ionomers. Although increasing the value of IEC can effectively improve the fuel cell performance, the formation of a distinct microphase separation morphology is viewed as a more important approach by numerous researchers because of the balance between the proton conductivity and mechanical properties.[16–19] And from the view of molecular design, a flexible sulfonated side-chain structure can facilitate the formation of a well-developed microphase separation morphology as well as construct a continuous hydrophilic ionic pathway, thus resulting in high performance and acceptable swelling.[20–22] Furthermore, ether-free backbones are considered a desired choice for prohibiting attack of hydroxyl radicals on ether bonds, which provides the fundamental support for achieving excellent membrane electrode assembly (MEA) durability.[23,24] Therefore, a series of synthetic methods used for the preparation of ether-free polymers, such as metal-catalyzed coupling reactions,[9] Diels–Alder polymerization[25] and superacid-catalyzed Friedel–Crafts polyhydroxyalkylation,[26–30] provide a significant platform for designing chemically stable ion exchange membranes.

Among these ether-free polyaromatic backbones, poly(arylene-alkane)s are a class of linear polymers prepared by efficient superacid-catalyzed Friedel–Crafts hydroxyalkylation. However, most poly(arylene-alkane)s are studied as anion exchange membranes (AEMs) due to the lack of sulfonation

aSchool of Physical Science and Technology, ShanghaiTech University, Shanghai 201210, China

bShanghai Advanced Research Institute, Chinese Academy of Sciences, Shanghai 201210, China. E-mail: qianhd@sari.ac.cn; yangh@sari.ac.cn

cUniversity of Chinese Academy of Sciences, Beijing 100049, China

This journal is © The Royal Society of Chemistry 2023

J. Mater. Chem. A, 2023, **11**, 4547–4558 | **4547**

methodology.[31–34] Facile and efficient sulfonation of poly(-phenyl-alkane)s remains a great challenge. In 2020, Pagels et al.[23] presented an effective and simple method of converting an alkyl halide functionality, a common precursor of AEMs,[35] to a sulfonate group. The Br– of bromoalkyl side chains was replaced by nucleophilic substitution with potassium thioacetate (KSAc), and then the thioacetate groups were converted to sulfonate groups using m-chloroperoxybenzoic acid (mCPBA) as the oxidant. This approach makes it possible to apply many ether-free polymers bearing a haloalkyl side chain to PEMs and provides inspiration for our work.

Besides, the compatibility of the membrane and ionomer with identical chemical structures plays a key role in boosting the performance and durability of MEAs, which can depress the charge transfer barrier and achieve high miscibility.[36] For example, Pu et al.[37] used a sulfonated poly(arylene ether ketone) material containing symmetrical tetramethyl groups (SPAEK-TM) as a membrane and ionomer to improve interfacial compatibility between PEMs and catalyst layers, which exhibited a higher power density compared to the Nafion ionomer in a direct methanol fuel cell and H$_2$/air fuel cell. Generally, ionomers are expected to dissolve in low-boiling-point protic solvents to avert adsorption of solvent residues on the catalyst surface, which can cover the electrochemically active site. However, many sulfonated aromatic polymers have a poor solubility in a mixture of water and alcohols, which limits their application in ionomers.

To date, a few researchers have studied fluorene as a backbone for ether-free AEMs due to its superior water vapor permeability and depressed the phenyl adsorption effect.[38,39] Yang et al.[39] introduced a series of poly[(fluorene alkylene)-co-(biphenyl alkylene)] (PFBA) AEMs, where a H$_2$/O$_2$ anion exchange membrane fuel cell (AEMFC) achieved a peak power density (PPD) of 0.559 W cm^{-2}. Chen et al.[33] reported an AEMFC based on poly(fluorenyl aryl piperidinium) (PFAP) membranes and ionomers that reached a PPD of 2.34 W cm^{-2} in a H$_2$/O$_2$ fuel cell. These results indicate that the fluorene segment in the polymers is beneficial for AEMs, which encourages us to explore the possibility of applying fluorene in ether-free aromatic PEMs.[40] Herein, we propose a series of poly(arylene-alkane)s (Poly(FLx-BPy)-SO$_3$H) as PEMs with a locally double sulfonated side-chain comb-like structure, which possesses denser ion clusters and higher IEC compared with conventional mono-sulfonated side-chain polymers. And the IEC values of PEMs can be simply adjusted via changing the proportion of monomers in copolymerization. By adopting the design of the combination of hydrophobic rigid ether-free hydrophobic main-chains and hydrophilic locally double sulfohexyl flexible side-chains, well-developed microphase separation and dense ion clusters or continuous channels are formed ultimately. Surprisingly, Poly(FLx-BPy)-SO$_3$H polymers exhibit favorable solubility in low-boiling-point solvents (e.g. alcohols), which provides a good opportunity to prepare ionomers in catalyst layers. As a benefit of rational structure design and the homogeneous membrane and ionomer, Poly(FLx-BPy)-SO$_3$H based MEAs exhibited desired high-performance and excellent durability compared to other state-of-the-art PEMs. The other properties of Poly(FLx-BPy)-SO$_3$H membranes with different sulfonation degrees (SDs) such as proton conductivity (σ), thermal stability, water uptake (WU), swelling ratio (SR) and oxidative stability will be studied systematically.

Experimental

Materials

Fluorene, 1,6-dibromohexane, biphenyl, dichloromethane, petroleum, methanol, trifluoromethanesulfonic acid (TFSA), N,N-dimethylacetamide (DMAc), N,N-dimethylformamide (DMF), dimethyl sulfoxide (DMSO), 1-Methyl-2-pyrrolidinone (NMP), N-propanol (NPA), isopropanol (IPA), potassium ethanethioate (KSAc), 3-chloroperoxybenzoic acid (85 wt%), and ethyl acetate were purchased from Adamas-beta. Sodium hydroxide, tetrabutylammonium iodide, sodium chloride, and sulfuric acid were obtained from China National Pharmaceutical Group Corporation (Shanghai, China). And all chemical reagents were directly used without further purification.

Synthesis of 9,9-bis(6-bromohexyl)-fluorene

The synthesis of 9,9-bis(6-bromohexyl)-fluorene was carried out following a procedure in the early literature (Scheme S1†).[41] Fluorene (16.00 g, 96.26 mmol) and tetrabutylammonium iodide (6.80 g, 18.41 mmol) were added to a three-necked flask. Then 40.00 g NaOH (1 mol) and 40.00 g water were mixed and poured into the flask. The mixture was stirred and refluxed at 70 °C in a nitrogen atmosphere for 48 h after 1,6-dibromohexane (90 mL) was added. Finally, the product was extracted with dichloromethane and purified using petroleum ether as an eluent by column chromatography. After vacuum drying, 24.02 g of 9,9-bis(6-bromohexyl)-fluorene was obtained (51% yield) as a viscous liquid.

Synthesis of Poly(FLx-BPy)-Br

The procedures of preparation of Poly(FLx-BPy)-Br are illustrated in Scheme 1. The synthesis of Poly(FL50-BP50)-Br was as follows: 9,9-bis(6-bromohexyl)-fluorene (2.4617 g, 5 mmol) and biphenyl (0.7710 g, 5 mmol) were dissolved with 8 mL anhydrous dichloromethane. Then 1,1,1-trifluoroacetone (1.46 g, 13 mmol) was added before TFSA (8.4 mL) was added dropwise over 5 min at 0 °C. After TFSA was added completely, the solution was warmed to room temperature and stirred for 60 min. Finally, the mixture was poured into methanol and a white precipitate was obtained. The polymer was filtered, washed subsequently with deionized water and dried to afford Poly(FL40-BP60)-Br (3.92 g, 94% yield).

Synthesis of Poly(FLx-BPy)-SAc

Taking the synthesis of Poly(FL50-BP50)-SAc as an example, Poly(FL50-BP50)-Br (3.52 g) and 40 mL DMAc were added into a flask. After the polymer was dissolved in DMAc, KSAc (1.926 g, 16.86 mmol) was placed into the flask. Then the mixture solution was stirred for 24 h at 50 °C. Finally, the reaction mixture was poured into methanol to obtain the product. The white
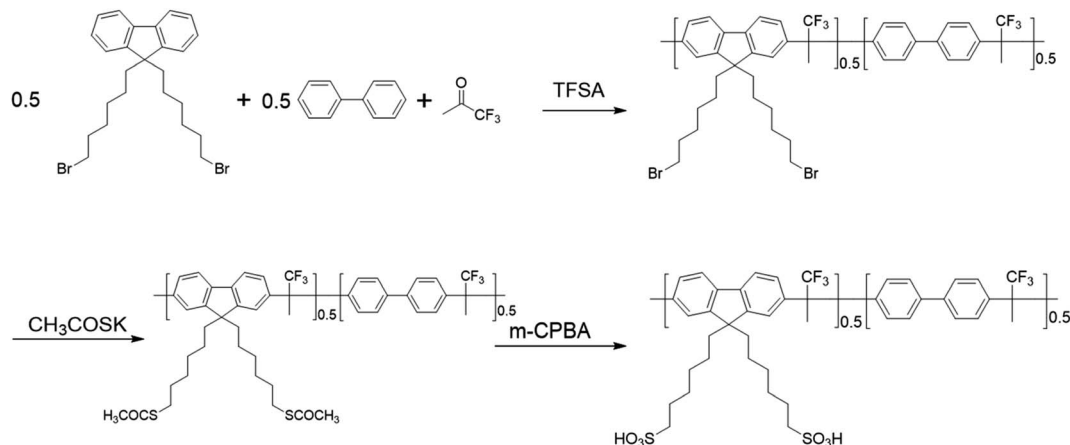
Scheme 1 Synthetic route of Poly(FL50-BP50)-SO₃H.

product was washed with methanol and dried in a vacuum for 24 h (3.21 g, 92% yield).

Synthesis of Poly(FLx-BPy)-SO₃Na

Taking the synthesis of Poly(FL50-BP50)-SO₃Na as an example, Poly(FL50-BP50)-SAc (3.8 g) was dissolved in 40 mL DMAc, and then 3-chloroperoxybenzoic acid (6.091 g, 30 mmol) was added at 0 °C. The reaction solution was warmed to room temperature and stirred for about 2 h, and eventually a gel-like solid was formed, locking the magneton without stirring. Then, the gel solid was taken out and placed in 1 M NaCl aqueous solution for precipitation. The resulting polymer was dissolved in DMSO and poured into ethyl acetate to complete purification twice. The purified polymer Poly(FL50-BP50)-SO₃Na was dried in a vacuum (3.43 g, 89% yield).

Preparation of Poly(FLx-BPy)-SO₃H membranes

Poly(FL50-BP50)-SO₃Na (1 g) and DMSO (20 mL) were mixed in a flask to form a 5 wt% polymer solution with continuous stirring at 60 °C. The solution was filtered and then cast onto a clean glass plate to evaporate solvent at 60 °C for 12 h. Then the polymer membrane was stripped from the glass plate and soaked in 1 M H₂SO₄ for 48 h to complete protonation to obtain Poly(FL50-BP50)-SO₃H.

Fabrication of MEAs and single cell performance

Poly(FL50-BP50)-SO₃H was dissolved in ethanol (5 wt%) at room temperature to prepare as the universal ionomer (the digital photograph is shown in Fig. S1†) for Poly(FLx-BPy)-SO₃H based MEAs. Then 0.100 g Pt/C (60 wt%, Johnson Matthey), 0.333 g water, and 2.500 g isopropyl were mixed with 0.222 g Poly(FL50-BP50)-SO₃H ionomer solution (5 wt%) by ultrasonication to acquire a homogeneous catalyst ink. The procedure for Nafion 212 based MEA is similar to that for Poly(FLx-BPy)-SO₃H except that the weight ratio of the Nafion ionomer and Pt/C was 1 : 4. The catalyst coated membranes (CCMs, the digital photograph is shown in Fig. S2†) were obtained using an air spray gun to deposit the ink on both sides of PEMs with an active electrode area of 2.5 × 2.5 cm² and the Pt loadings for the anode and cathode were both 0.2 mg cm⁻². Finally, the CCMs were sandwiched between the cathode and anode gas diffusion electrodes (GDEs, Sigracet 22 BB, SGL Carbon) to manufacture the MEAs. The fuel cell performance was evaluated using an Arbin fuel cell testing system (Arbin Instrument Inc., USA) with H₂ (400 sccm) and air (1000 sccm) or O₂ (400 sccm) at 100% RH and under 2 bar backpressure at 80 °C.

Characterization

¹H NMR spectra and ¹⁹F NMR spectra of the polymers were obtained on a Bruker AV500 spectrometer. Tensile strength and the break elongation rate of PEMs were obtained on a universal testing machine (Instron-5966, USA) under environmental conditions with a speed of 1 mm min⁻¹. A Mettler-Toledo TGA/DSC 3+/1100 LF analyzer was used to conduct thermogravimetric analysis (TGA) of polymers before and after sulfonation under a N₂ flow from 50 to 800 °C (10 °C min⁻¹). The transmission electron microscopy (TEM) images and small angle X-ray scattering (SAXS) profiles of PEMs were obtained on a JEM-1400 plus and SAXSess mc2 after the membranes were dyed with Pb(OAc)₂·3H₂O. A scanning electron microscope (SEM, Phenom Prox) was applied to observe surface morphology of the four PEMs and cross-sectional morphology of the MEA fabricated with the Poly(FL50-BP50)-SO₃H membrane before and after the durability test. The molecular weight of Poly(FL50-BP50)-SO₃H before and after the durability test was acquired by gel permeation chromatography (GPC, Waters GPC 1515) using DMF as an eluent with a flow rate of 1 mL min⁻¹. The proton conductivity (σ) was obtained using a Solartron Analytical 1260 and 1287 using the following equation: σ (S cm⁻¹) = L/RWd, where R represents the resistance of the membrane surveyed by four-point probe AC impedance spectroscopy over the frequency range of 10⁶ to 1 Hz with a disturbance potential of 10 mV, L is the length of the two electrodes, and W and d are the width and thickness of the membrane, respectively. Electrochemical impedance spectroscopy (EIS) was conducted at 200 mA cm⁻² with 5 mA cm⁻² amplitude of the AC signal over the frequency range of 10⁶ to 1 Hz. Linear sweep voltammetry (LSV) experiments were conducted

This journal is © The Royal Society of Chemistry 2023

J. Mater. Chem. A, 2023, **11**, 4547–4558 | **4549**

to evaluate the H_2 crossover with a humidified H_2 flow rate of 400 sccm at the anode and humidified N_2 flow rate of 400 sccm at the cathode. The cathode (working electrode) potential was scanned from 0.05 to 0.5 V with a rate of 5 mV s^{-1} at 80 °C. The anode served as the reference and counter electrodes. The H_2 crossover current of the MEAs was calculated from the current at 0.4 V in the LSV curves. And the specific test methods for the proton conductivity, the water uptake (WU), swelling ratio (SR), oxidative stability and ion exchange capacity (IEC) are shown in our previous report.[4]

Results and discussion

Synthesis of Poly(FLx-BPy)-SO$_3$H

As shown in Scheme 1, the –Br groups on the side chains of Poly(FL50-BP50)-Br are replaced by –SAc via a nucleophilic substitution reaction, and then the –SAc of Poly(FL50-BP50)-SAc can be easily oxidized to sulfonate groups with 3-chloroperoxybenzoic acid. As shown in Fig. 1, after the –Br is replaced by –SAc, the peak of H_l shifts to the higher field and appears at $\delta = 2.71$ ppm (H_l in poly(FL50-BP50)-SAc), while a new peak of H_m appears at 2.25 ppm, thus marking the completion of the substitution. And after further sulfonation, the peak of H_m disappears and the chemical shift value of H_l migrates to 2.454 ppm (H_l in Poly(FL50-BP50)-SO$_3$H), demonstrating the completion of the sulfonation process. Besides, the ^{19}F NMR spectra of Poly(FLx-BPy)-SO$_3$H (Fig. 2a) have only one peak and the corresponding chemical shift values remain constant, indicating the high purity of the polymers. The ^{1}H NMR spectra of other polymers can be seen in Fig. S3–S5.†

Furthermore, the FT-IR spectra (Fig. 2b and S6–S8†) also confirm the successful sulfonation process of polymers; the C–Br
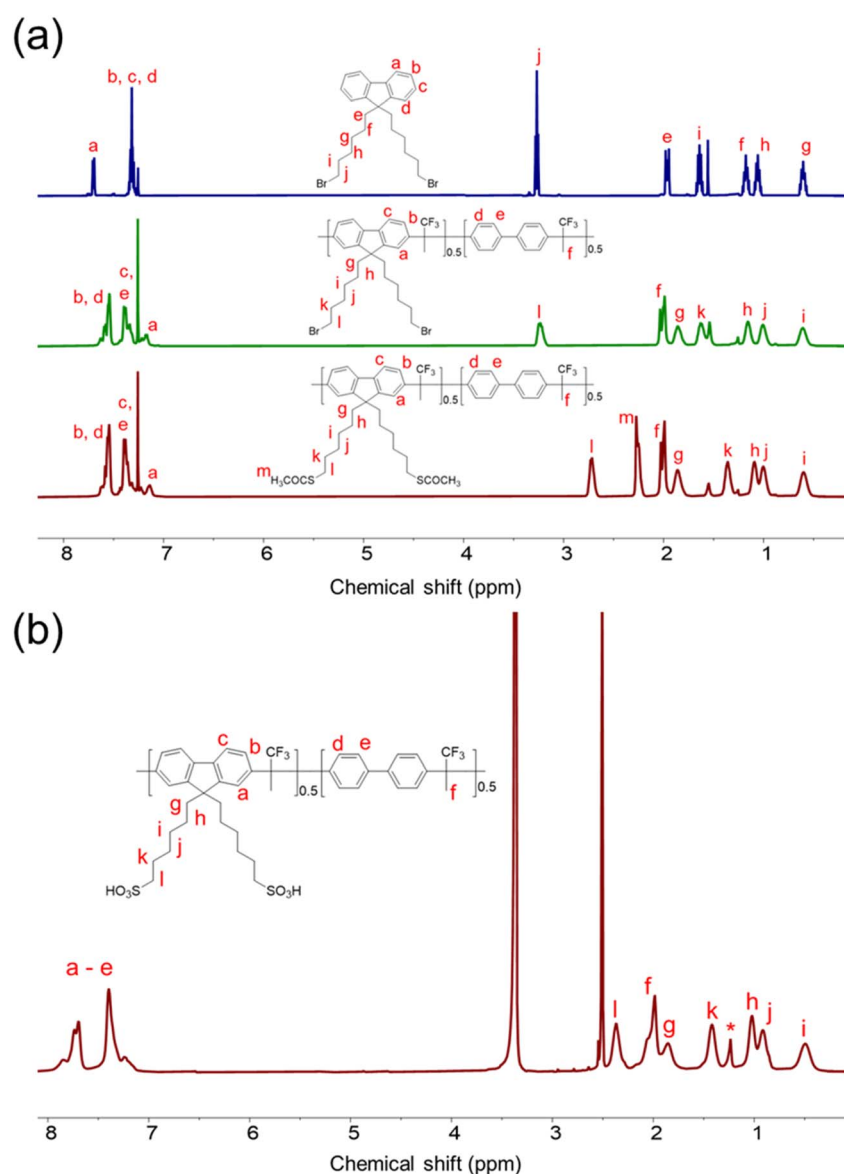
Fig. 1 (a) ^{1}H NMR spectra of 9,9-bis(6-bromohexyl)-fluorene and Poly(FL50-BP50)-Br and Poly(FL50-BP50)-SAc in CDCl$_3$, and (b) ^{1}H NMR spectra of Poly(FL50-BP50)-SO$_3$H in DMSO-d_6 (* = vacuum grease).

4550 | J. Mater. Chem. A, 2023, 11, 4547–4558

This journal is © The Royal Society of Chemistry 2023
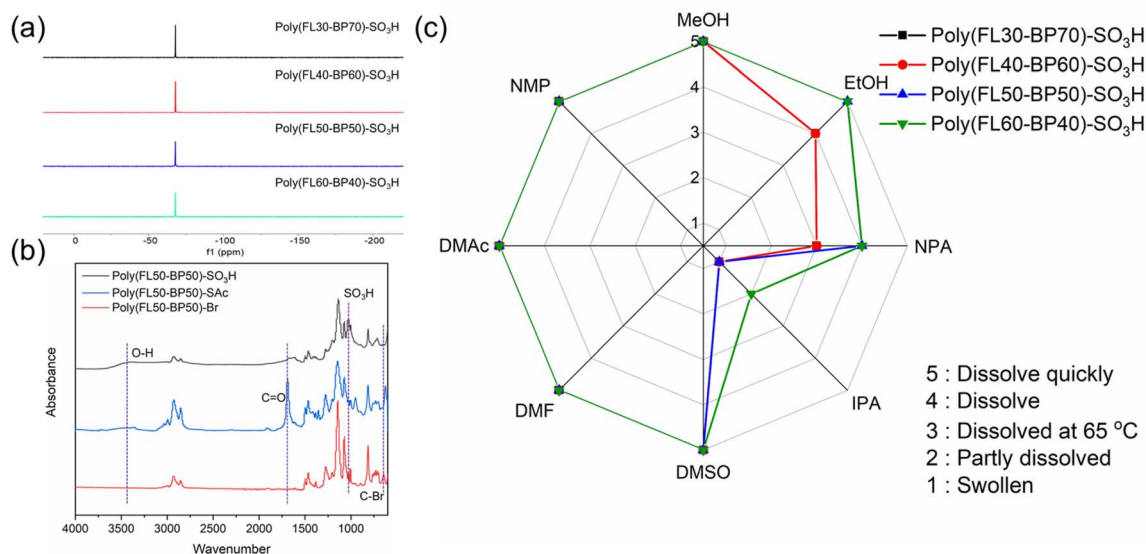
Fig. 2 (a) ^{19}F NMR spectra of Poly(FLx-BPy)-SO$_3$H in DMSO-d_6. (b) FT-IR spectra of Poly(FL50-BP50)-Br, Poly(FL50-BP50)-SAc and Poly(FL50-BP50)-SO$_3$H. (c) Solubility properties of Poly(FLx-BPy)-SO$_3$H.

characteristic absorption peak at 643 cm^{-1} of Poly(FL50-BP50)-Br disappears, while the sharp absorption peak at 1690 cm^{-1} which originated from C=O of –SAc appears in Poly(FL50-BP50)-SAc spectra. Finally, the wide stretching vibration absorption peak at 3400 cm^{-1} of the O–H moiety and new peaks at 1072 and 1026 cm^{-1} of sulfonic acid groups of Poly(FL50-BPy-50)-SO$_3$H increase in intensity. Fig. 2c presents the solubility difference of Poly(FLx-BPy)-SO$_3$H. Poly(FLx-BPy)-SO$_3$H membranes can be dissolved in most solvents mentioned in the radar chart and exhibit higher solubility as the SD. Surprisingly, Poly(FLx-BPy)-SO$_3$H polymers exhibit favorable solubility in alcohol, which provides a good opportunity to prepare ionomers in catalyst layers, contributing to improving the performance of PEMFCs.

Thermogravimetric analysis

In general, sufficient thermal stability is necessary for PEMs in practical applications. Fig. 3a and b exhibit the TGA profiles of the pre- *versus* post- sulfonated polymers from 50 to 800 °C

under a N$_2$ flow. The degradation paths of the four pre-sulfonated Poly(FLx-BPy)-Br polymers are consistent. The four pre-sulfonated polymers show the standard two-stage degradation pathway. The first stage from 340 to 503 °C is the thermal decomposition of the bromoalkyl side-chains, and the mass losses at this stage gradually increase with the bromoalkyl content. Besides, the second weight losses at >530 °C primarily originated from thermal degradation of the polymer main-chains.

The weight varying curves of the four PEMs mainly fall into three stages. In the range of 50 to 240 °C, all four PEMs have a small but varying degree of mass loss, which should be attributed to residual water within the Poly(FLx-BPy)-SO$_3$H membranes. Moreover, an interesting phenomenon is that the mass losses of Poly(FLx-BPy)-SO$_3$H membranes at this stage increase with the SD. The mass losses in the second section from 240 to 530 °C are mainly due to the decomposition of the sulfonation groups and the alkyl side-chains, which is similar to
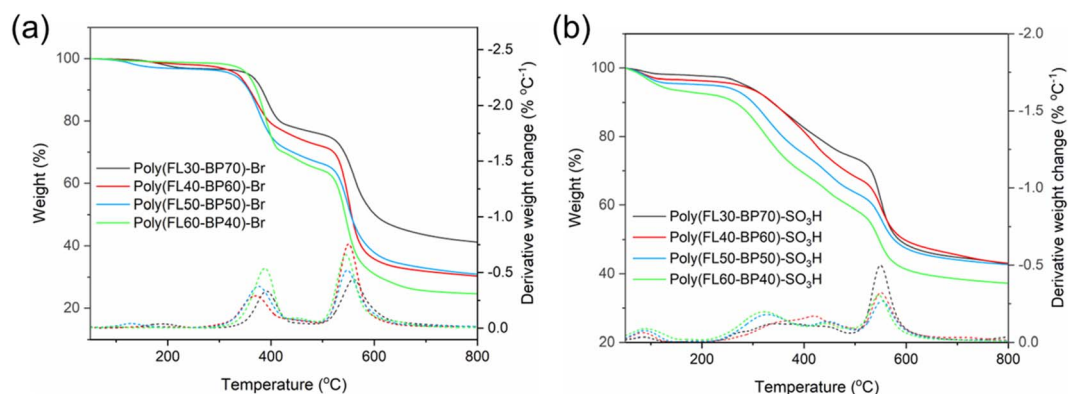
Fig. 3 TGA curves in a N$_2$ flow from 50 to 800 °C of (a) Poly(FLx-BPy)-Br and (b) Poly(FLx-BPy)-SO$_3$H.

This journal is © The Royal Society of Chemistry 2023

J. Mater. Chem. A, 2023, **11**, 4547–4558 | **4551**

the characteristics exhibited in the first stage; the mass losses of this period improve with the SD. The section above 530 °C belongs to the third period, where mass losses are primarily caused by the degradation of the polymer backbone.

Proton conductivity, water uptake and swelling ratio

High proton conductivity is a vital index for PEMs. The proton conductivity of the four PEMs prepared in this work can be seen in Fig. 4a. Benefiting from the comb-like structure and high IEC (Table 1), Poly(FLx-BPy)-SO$_3$H membranes all possess a high σ that provides outstanding power density. Poly(FL50-BP50)-SO$_3$H (0.106 S cm^{-1} at 25 °C and 0.191 S cm^{-1} at 80 °C) and Poly(FL60-

BP40)-SO$_3$H (0.115 S cm^{-1} at 25 °C and 0.202 S cm^{-1} at 80 °C) membranes exhibit obviously higher σ compared to Poly(FL30-BP70)-SO$_3$H (0.064 S cm^{-1} at 25 °C and 0.134 S cm^{-1} at 80 °C) and Poly(FL40-BP60)-SO$_3$H (0.076 S cm^{-1} at 25 °C and 0.160 S cm^{-1} at 80 °C) due to the formation of continuous hydrophilic ion channels. Besides, the proton conduction activation energy (E_a) calculated with Arrhenius plots of Poly(FLx-BPy)-SO$_3$H (Fig. S9†) is found to be in the range of 8.8–11.9 kJ mol^{-1} with a tendency of lower E_a for higher SD, indicating the enhanced proton conduction capacity with the increased SD. The WU (Fig. 4c) and SR (Fig. 4d) of the prepared Poly(FLx-BPy)-SO$_3$H membranes were measured from 25 to 80 °C; Poly(FLx-BPy)-SO$_3$H membranes have a high WU (47–91% at 80 °C) in liquid
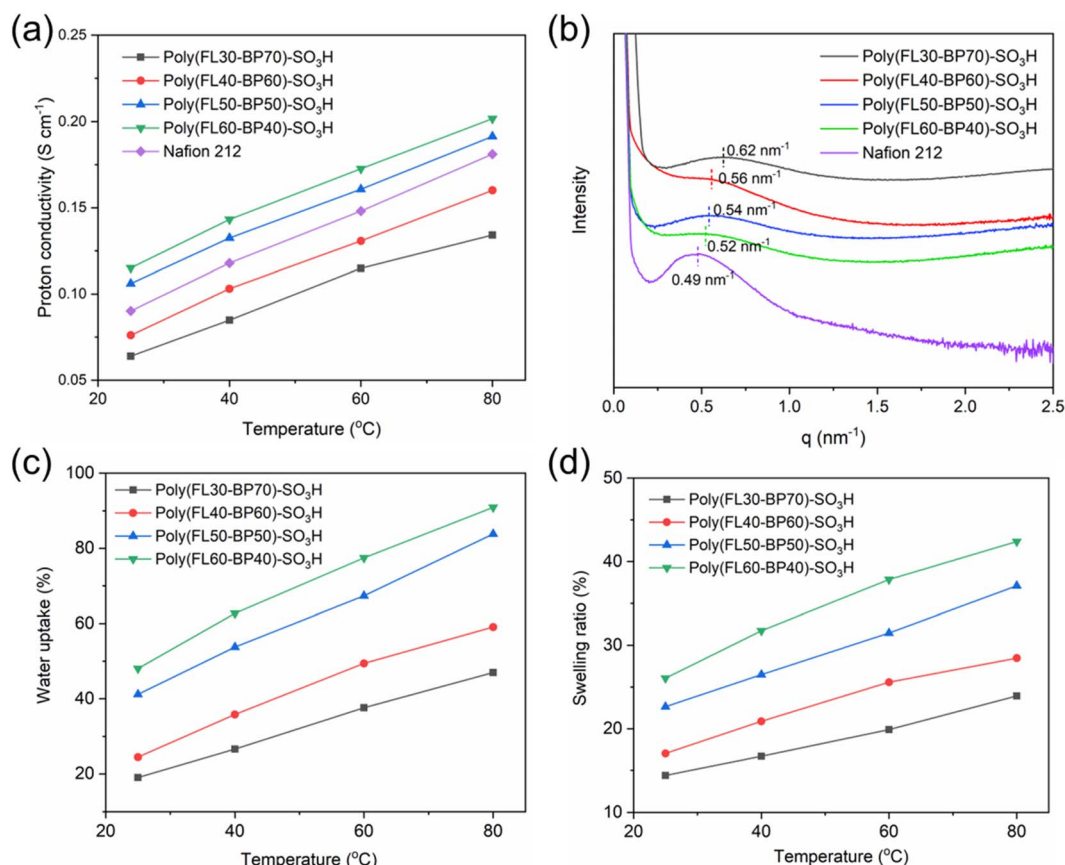
Fig. 4 (a) Proton conductivity of Poly(FLx-BPy)-SO$_3$H membranes as a function of temperature. (b) SAXS profiles of Poly(FLx-BPy)-SO$_3$H and Nafion 212. (c) Water uptake and (d) swelling ratio of Poly(FLx-BPy)-SO$_3$H membranes as a function of temperature.

Table 1 Mechanical properties, oxidative stabilities and IEC of PEMs

PEMs	Tensile strength (MPa)	Young's modulus (MPa)	Elongation at break (%)	Residual weight[a] (%)	Theoretical IEC[b] (meq g^{-1})	Titrated IEC[c] (meq g^{-1})
Poly(FL30-BP70)-SO$_3$H	37.9	894	6.5	99.6	1.71	1.64
Poly(FL40-BP60)-SO$_3$H	39.5	1169	4.8	99.5	2.08	1.93
Poly(FL50-BP50)-SO$_3$H	49.1	1177	4.5	99.5	2.39	2.21
Poly(FL60-BP40)-SO$_3$H	51.6	1189	4.1	99.4	2.65	2.54

[a] Residual weight of Poly(FLx-BPy)-SO$_3$H under Fenton's reagent at 80 °C for 4 h. [b] Theoretical IEC was calculated from the integration of ^{1}H NMR spectra. [c] Titrated IEC was calculated by titration with 0.01 M NaOH using phenolphthalein as the indicator. Before titration, the membranes were immersed into 1 M NaCl solution for 24 h to promote the ion exchange.

4552 | J. Mater. Chem. A, 2023, **11**, 4547–4558

This journal is © The Royal Society of Chemistry 2023

water, while Poly(FLx-BPy)-SO$_3$H displays a moderate SR (24–42% at 80 °C) with a trend of higher WU and SR for higher SD. These data reveal that the combination of rigid ether-free hydrophobic main-chains and a locally double sulfohexyl side-chains comb-like structure improves σ and dimensional stability of Poly(FLx-BPy)-SO$_3$H.

Mechanical properties and oxidative stability

To meet the actual application, the PEMs must have enough mechanical strength and oxidation resistance.[42] Related mechanical properties and the oxidative stability data are summarized in Table 1, and the stress–strain curves of Poly(FLx-BPy)-SO$_3$H membranes can be seen in Fig. S10.† As presented in Table 1, the tensile strength and Young's modulus of Poly(FLx-BPy)-SO$_3$H are in the sequence of Poly(FL60-BP40)-SO$_3$H (51.6 MPa and 1189 MPa) > Poly(FL50-BP50)-SO$_3$H (49.1 MPa and 1177 MPa) > Poly(FL40-BP60)-SO$_3$H (39.5 MPa and 1169 MPa) > Poly(FL30-BP70)-SO$_3$H (37.9 MPa and 894 MPa). Meanwhile, the break elongation follows the order of Poly(FL60-BP40)-SO$_3$H (4.1%) < Poly(FL50-BP50)-SO$_3$H (4.5%) < Poly(FL40-BP60)-SO$_3$H (4.8%) < Poly(FL30-BP70)-SO$_3$H (6.5%) as a result of reduced fluorene content and polymer rigidity.

Preeminent oxidative stability is essential for the practical application of PEMs. The PEMs were immersed in Fenton's reagent at 80 °C for 4 h to test their oxidative stability. As a benefit of the ether-free polyaromatic backbone, the Poly(FLx-BPy)-SO$_3$H membranes remained intact and the residual weight ranged above 99% (Table 1) after the test, which provided fundamental support for the durability of the corresponding MEA.

Morphology

In general, it is of great significance to form distinct microphase separation morphology within PEMs, because it will remarkably enhance the proton conduction capacity and help to contain swelling.[43] Herein, the TEM characterization of Poly(FLx-BPy)-SO$_3$H was performed and is shown in Fig. 5; the bright region represented the hydrophobic section and the dark region represented the hydrophilic portion formed by the ionic clusters. When the SD increases from 30% to 40%, the density of hydrophilic ion clusters gradually improves, and when the SD increases from 40% to 50%, the hydrophilic ion clusters begin to aggregate to form continuous hydrophilic ion channels, which will help to further enhance its proton conductivity as well as water uptake. Ultimately, as the SD improves from 50% to 60%, the degree of continuity and size of hydrophilic ion channels increase ulteriorly due to the agglomeration of more sulfonic acid groups. Besides, the microphase separation morphology in Poly(FLx-BPy)-SO$_3$H was further verified by SAXS. The sizes of the ion clusters or channels calculated using SAXS profiles (Fig. 4b) are approximately 10.1, 11.2, 11.6, 12.1 and 12.8 nm for Poly(FL30-BP70)-SO$_3$H, Poly(FL40-BP60)-SO$_3$H,
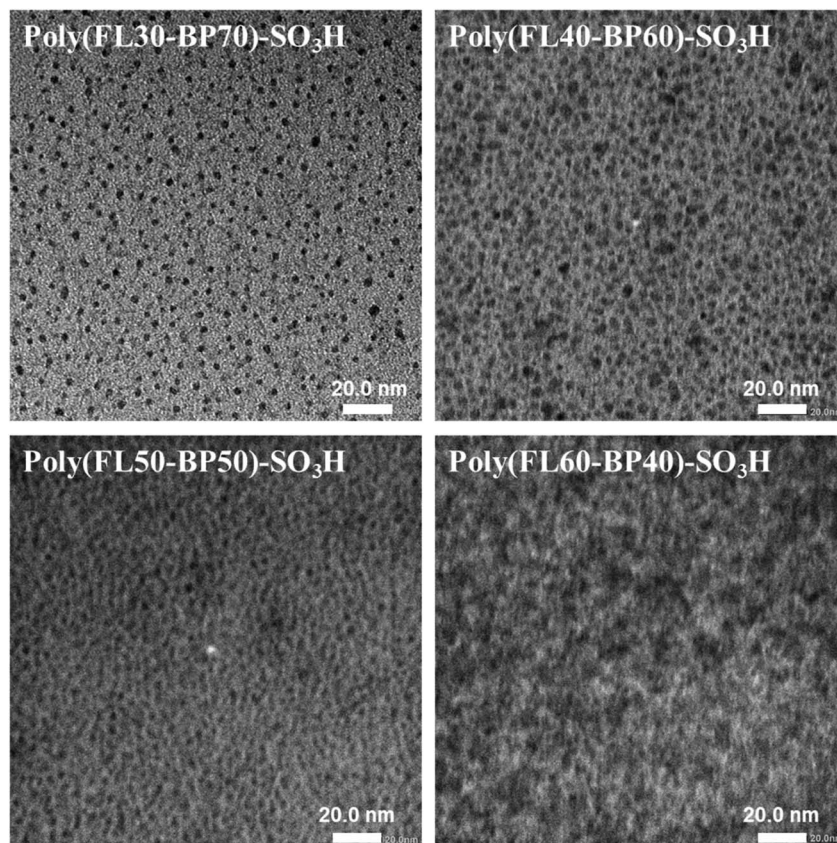
Fig. 5 TEM images of Poly(FLx-BPy)-SO$_3$H membranes stained with Pb(OAc)$_2$.

This journal is © The Royal Society of Chemistry 2023

J. Mater. Chem. A, 2023, **11**, 4547–4558 | **4553**

Poly(FL50-BP50)-SO$_3$H, Poly(FL60-BP40)-SO$_3$H and Nafion 212, respectively. Both TEM and SAXS data certify that well-developed microphase separation is formed in Poly(FLx-BPy)-SO$_3$H with the hydrophilic flexible side chains. Thereinto, Poly(FL50-BP50)-SO$_3$H and Poly(FL60-BP40)-SO$_3$H possess continuous hydrophilic ion channels.

Fuel cell performance

To estimate the feasibility of the prepared membranes in PEMFCs, the performance of MEAs integrated with Poly(FLx-BPy)-SO$_3$H and Nafion 212 was tested under H$_2$/air or H$_2$/O$_2$ conditions. Considering the good solubility in alcohols or the mixture of alcohols with water, high proton conductivity, and dimensional stability in hot water, we selected Poly(FL50-BP50)-SO$_3$H as the universal ionomer for Poly(FLx-BPy)-SO$_3$H based MEAs. Fig. 6a and b show the polarization and power density curves of the MEAs with 100% RH H$_2$ and air or O$_2$ under 2 bar backpressure at 80 °C. The open-circuit voltages (OCVs) of Poly(FLx-BPy)-SO$_3$H are 0.967–0.987 V for H$_2$/air and 1.016–1.036 V for H$_2$/O$_2$, slightly lower than that of the Nafion 212 based MEA (0.957 V for H$_2$/air and 1.013 V for H$_2$/O$_2$) (Table S1†), suggesting the low H$_2$ permeability of Poly(FLx-BPy)-SO$_3$H membranes. The PPD of MEAs is in the order of Poly(FL50-BP50)-SO$_3$H (MEA3, 1.108 W cm^{-2} for H$_2$/air and 2.465 W cm^{-2} for H$_2$/O$_2$) > Poly(FL60-BP40)-SO$_3$H (MEA4, 1.070 W cm^{-2} for

H$_2$/air and 2.242 W cm^{-2} for H$_2$/O$_2$) > Nafion 212 (MEA5, 0.992 W cm^{-2} for H$_2$/air and 2.080 W cm^{-2} for H$_2$/O$_2$) > Poly(FL40-BP60)-SO$_3$H (MEA2, 0.916 W cm^{-2} for H$_2$/air and 1.915 W cm^{-2} for H$_2$/O$_2$) > Poly(FL30-BP70)-SO$_3$H (MEA1, 0.837 W cm^{-2} for H$_2$/air and 1.668 W cm^{-2} for H$_2$/O$_2$). Although Poly(FL60-BP40)-SO$_3$H has a higher proton conductivity than Poly(FL50-BP50)-SO$_3$H, MEA4 does not display expected fuel cell performance but MEA3 delivers one of the best performances in PEMFCs as compared with recent publications (Table S2†). Poly(FL60-BP40)-SO$_3$H has a higher IEC than Poly(FL50-BP50)-SO$_3$H, which is accompanied by a significant increase in water uptake and dimensional swelling, loss in mechanical strength, or even deterioration of the MEA at elevated temperatures. Besides, the subtle incompatibility of the Poly(FL60-BP40)-SO$_3$H membrane and Poly(FL50-BP50)-SO$_3$H ionomer also leads to the performance deterioration of MEA4. This result confirms that relatively high content of sulfohexyl groups and high miscibility of membranes with ionomers are beneficial for the fuel cell performance.

Furthermore, the H$_2$ permeability of MEA1-5 was calculated by using the linear sweep voltammograms (LSVs) with H$_2$ and N$_2$ for the anode and cathode at 80 °C and 100% RH. As shown in Fig. 6c, the H$_2$ crossover current densities of MEA1-4 are 0.986, 0.862, 0.755 and 0.554 mA cm^{-2}, respectively, which are lower than that of MEA5 (1.827 mA cm^{-2}) and in line with the trend of OCVs. It is noticeable that the sulfoalkyl-tethered
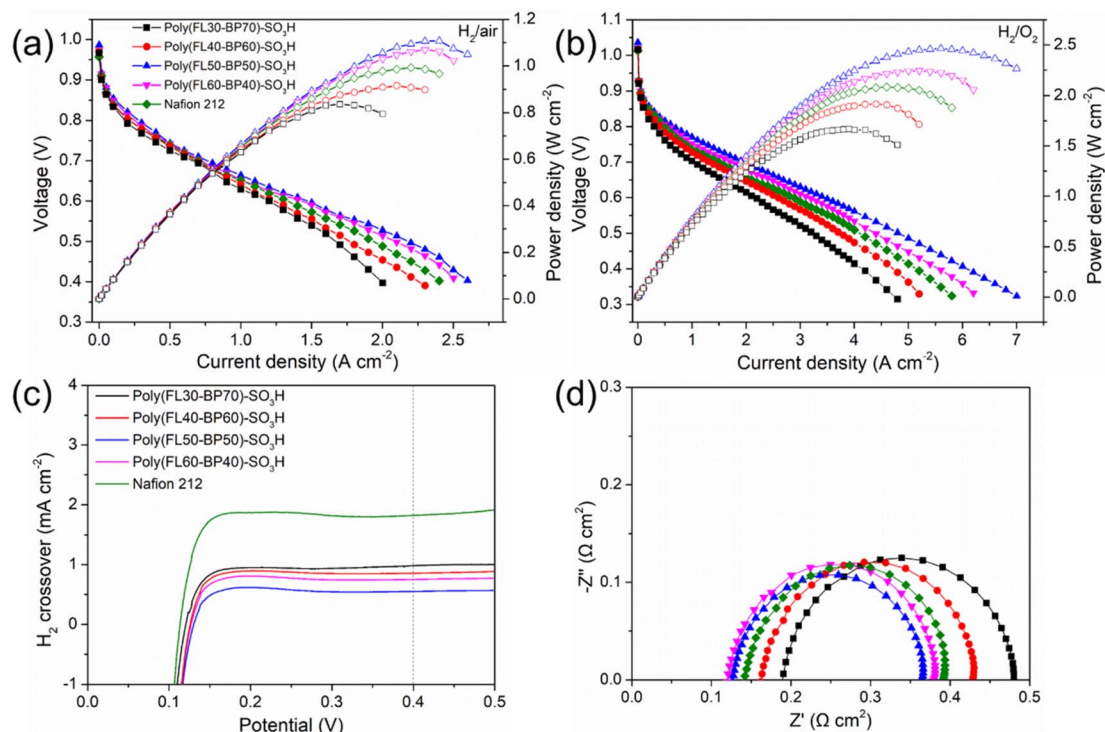
Fig. 6 Steady-state polarization curves of MEAs fabricated with Poly(FLx-BPy)-SO$_3$H and Nafion 212 under (a) H$_2$/air and (b) H$_2$/O$_2$. Test conditions: 80 °C with H$_2$ (400 sccm) and air (1000 sccm) or O$_2$ (400 sccm) at 100% RH and 2 bar backpressure; Pt loadings for the anode and cathode were both 0.2 mg cm^{-2}. (c) Linear sweep voltammograms of various MEAs. Test conditions: 100%RH H$_2$ (400 sccm) and N$_2$ (400 sccm) without backpressure and a scan rate of 5 mV s^{-1} at 80 °C. The value at 0.4 V represents the current density of H$_2$ crossover through the CCM. (d) EIS data of various MEAs. Test conditions: 80 °C at 200 mA cm^{-2} with 5 mA cm^{-2} amplitude of the AC signal over the frequency range of 10^6 to 1 Hz.

4554 | J. Mater. Chem. A, 2023, 11, 4547–4558

This journal is © The Royal Society of Chemistry 2023

polymers possess a smooth and imperforate surface (Fig. S11†) as well as a dense structure and the higher the content of the densely sulfonated structure the greater the barrier function for hydrogen permeation.

The Nyquist plot obtained at 0.2 A cm^{-2} ($\sim$0.8 V, kinetic region) consists of one semicircle that reflects the charge transfer resistance (R_{CT}). In the kinetic region, the main contribution of R_{CT} arises from the cathodic oxygen reduction reaction (ORR). The real axis intercept indicates the ohmic resistance of the MEA (R_{Ω}), which is the sum of (a) ionic resistance within the electrolytes, (b) electronic resistance within the cell's hardware, and (c) contact resistance within the inter connections.[44] It can be observed in Fig. 6d that as the SD increases, the R_{Ω} of Poly(FLx-BPy)-SO$_3$H based MEAs decreases from 0.189 to 0.120 Ω cm^2, whereas the value for the MEA fabricated with Nafion 212 and the Nafion ionomer (MEA5) is 0.141 Ω cm^2. In general, a huge proportion of R_{Ω} is mainly caused by the ion migration resistance of the membrane under operating conditions. Accordingly, this result is in agreement with the proton conductivity of the PEMs.

Different from trend of R_{Ω}, the R_{CT} of Poly(FLx-BPy)-SO$_3$H based MEAs is in the range of 0.237 to 0.291 Ω cm^2, and the Poly(FL50-BP50)-SO$_3$H based MEA (MEA3) possesses the lowest R_{CT}. The subtle difference originates from the favorable compatibility between the Poly(FL50-BP50)-SO$_3$H membrane and the Poly(FL50-BP50)-SO$_3$H ionomer. As a result, MEA4, consisting of the Poly(FL60-BP40)-SO$_3$H membrane and Poly(FL50-BP50)-SO$_3$H ionomer, exhibits a higher R_{CT} (0.260 Ω cm^2) than MEA3 (0.237 Ω cm^2). The R_{CT} of MEA5 is 0.251 Ω cm^2, higher than that of MEA3, but lower than that of the MEA fabricated with Poly(FL30-BP70)-SO$_3$H (MEA1, 0.291 Ω cm^2) and Poly(FL40-BP60)-SO$_3$H (MEA2, 0.266 Ω cm^2), suggesting the high electrochemical activity of homogeneous MEA featuring high proton conductivity and identical chemical structure of the membrane and ionomer.

To further evaluate the compatibility of the PEMs and ionomers, the mass activities (MAs) of the Poly(FL50-BP50)-SO$_3$H bonded electrode for Poly(FLx-BPy)-SO$_3$H and Nafion bonded MEA of Nafion 212 were calculated from the current density at 0.9 V and cathodic Pt loading (Fig. S12†). MEA3 exhibits the highest MA with a value of 0.165 A mg^{-1} for H$_2$/air and 0.281 A mg^{-1} for H$_2$/O$_2$, indicating the boosted Pt utilization efficiency for the ORR. Besides, the MA of MEA4 (0.156 A mg^{-1} for H$_2$/air and 0.254 A mg^{-1} for H$_2$/O$_2$) is also higher than that of the Nafion one (0.122 A mg^{-1} for H$_2$/air and 0.230 A mg^{-1} for H$_2$/O$_2$) while the values for MEA1 (0.084 A mg^{-1} for H$_2$/air and 0.171 A mg^{-1} for H$_2$/O$_2$) and MEA2 (0.096 A mg^{-1} for H$_2$/air and 0.207 A mg^{-1} for H$_2$/O$_2$) are lower than that of MEA5, consistent with the trend of the above proton conductivity results. Consequently, the high proton conductivity of the PEMs is favorable to enhance intrinsic activity towards the ORR and the Poly(FL50-BP50)-SO$_3$H membrane is more compatible with identical ionomers in the catalyst layers.

Durability is an extremely important indicator to evaluate the practical application potential of PEMs. Taking the high performance of Poly(FL50-BP50)-SO$_3$H into account, MEA3 was used for the durability test at a constant current density of 0.5 A

cm^{-2} (Fig. 7a). In the first 36 h, the voltage drops rapidly from the initial 0.750 V to 0.684 V with a voltage decay rate of 1.83 mV h^{-1}. Then the voltage drops slightly from 0.684 V to 0.510 V with a decay rate of 0.48 mV h^{-1}. The durability of MEA3 is one of the highest compared to other recent reports (Table S2†).

The decay in voltage of MEAs might be caused by cathode flooding, platinum oxidation, degradation of the membrane and ionomer, contaminant adsorption, etc.[45] The detailed reasons need to be further explored. During the durability measurement of MEA3, several restarts were experienced to regain recoverable performance. As shown in Fig. 7b, the H$_2$ crossover current density increases with time, where the value after 171, 306 and 400 h increases by 114%, 173% and 280%, respectively.

The EIS test was further conducted to get insight into the degradation of MEA3. It can be seen in Fig. 7c that both the real axis intercept and diameter of each impedance semicircle increase with time. From 171 to 400 h, the R_{Ω} of the Poly(FL50-BP50)-SO$_3$H based MEA increases by 42.5–149.6% while the R_{CT} increases by 6.3–48.5%.Besides, the relative change in H$_2$ crossover (280%) before and after the durability test demonstrates much larger variation than the relative change in R_{CT} (48.5%), indicating that the voltage loss mainly arises from the degradation of the proton pathway within the membrane.

After the durability test, MEA3 was disassembled, and Poly(FL50-BP50)-SO$_3$H was carefully recovered by dissolving the MEA fragments into DMSO for post-test analyses. Then the chemical degradation of the membrane was studied by GPC and NMR techniques. As shown in Fig. 7d, GPC analyses suggest a loss in the molecular weight from a number-average molecular weight (M_n) of 73 kDa and weight-average molecular weight (M_w) of 108 kDa for the pristine PEM to M_n = 61 kDa and M_w = 96 kDa for the recovered PEM. The M_w decreases by 11% while the polydispersity index (PDI) increases slightly from 1.48 to 1.57, indicating that the loss is dominated by the degradation of sulfonic acid groups, rather than the ether-free polymer backbone because the degradation of the polymer backbone will lead to an evident increase in the PDI. Besides, the ^{1}H and ^{19}F NMR spectra (Fig. S13†) of the post-test membrane also display minor differences in the chemical structure, further confirming the durability of the ether-free main chain in the Poly(FL50-BP50)-SO$_3$H membrane under operating conditions.

The cross-section morphology of MEA3 before and after the durability test was investigated to evaluate the strength of catalyst layers/membrane layers. As shown in Fig. 7e, the thickness of the catalyst layers (anode or cathode) and membrane layer of the original MEA is $\sim$2.4 and $\sim$31.5 μm, respectively. After 400 h of operation, the thickness of the three layers decreases slightly and there is no delamination or rupture at the interfaces. The great durability of interfaces can be attributed to two reasons: (1) the high chemical stability of the ether-free polymer backbone and (2) high interfacial compatibility with the membrane and identical ionomer in the catalyst layers. These results also support that the voltage loss mainly arises from the PEMs rather than the catalyst layers and the slight drop in M_w would cause great changes in the proton conduction within the MEA.

This journal is © The Royal Society of Chemistry 2023

J. Mater. Chem. A, 2023, 11, 4547–4558 | **4555**
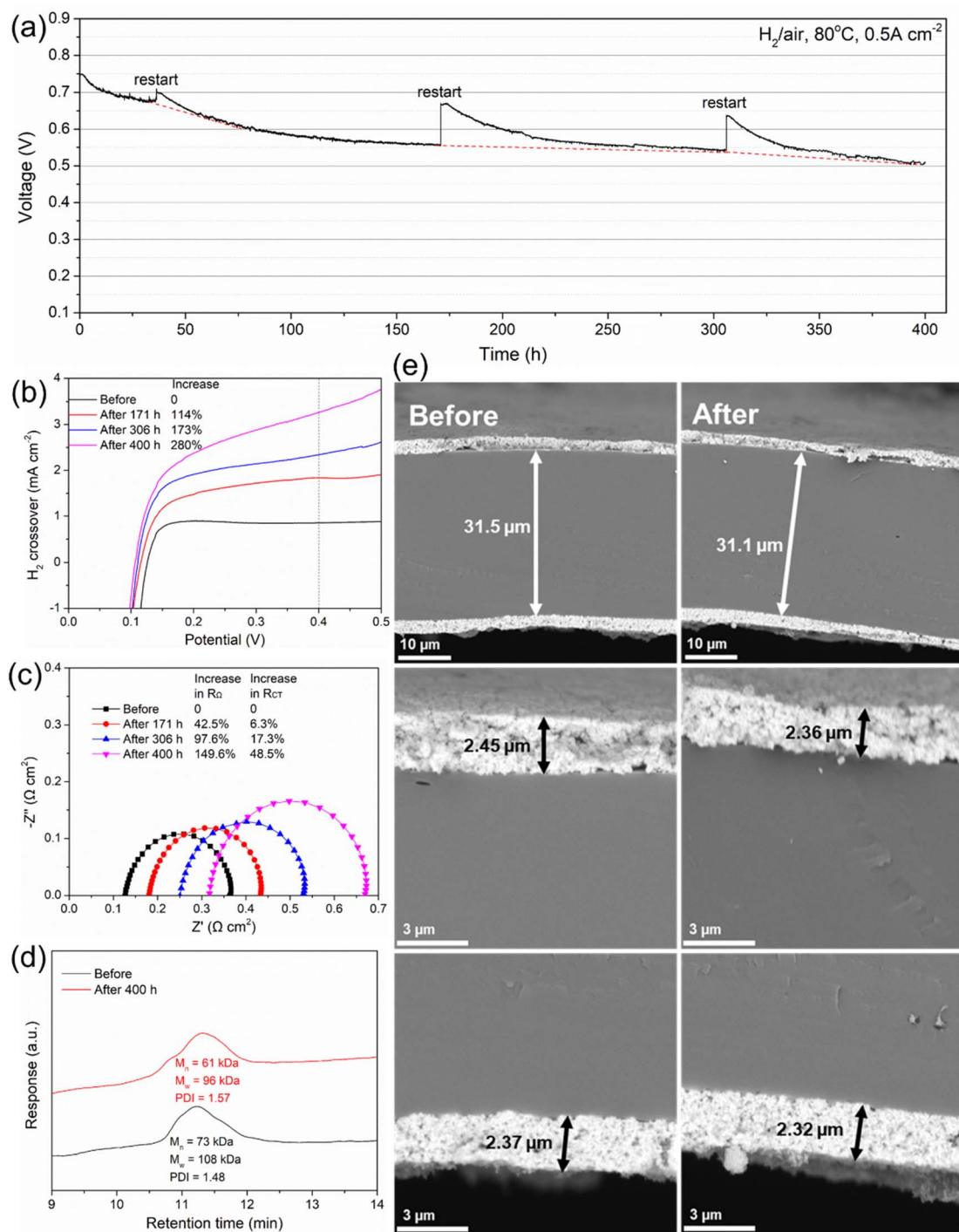
Fig. 7 Durability analyses of MEA3. (a) Discharging curve of MEA3 at a constant current density of 0.5 A cm^{-2} with supplying H$_2$ and air for 400 h. Test conditions: 80 °C with H$_2$ (400 sccm) and air (1000 sccm) at 100% RH and 2 bar backpressure; Pt loadings for the anode and cathode were both 0.2 mg cm^{-2}. (b) LSV and (c) EIS data of MEA3 before and after durability tests of 171 h, 306 h and 400 h. The relative changes in H$_2$ crossover, and R_Ω and R_{CT} included in the figures indicate that the voltage loss mainly arises from the PEM. (d) GPC profiles of Poly(FL50-BP50)-SO$_3$H before and after the durability test using the DMF eluent. (e) SEM images of cross-section morphology of MEA3 before (left) and after (right) the durability test.

Conclusions

In this work, a series of high-performance ether-free Poly(FLx-BPy)-SO$_3$H polymers with a locally double sulfonated side-chain comb-like structure have been proposed. The ether-free aromatic backbones provide the fundamental support for achieving excellent MEA stability. The comb-like structure results in well-developed microphase separation morphology.

4556 | J. Mater. Chem. A, 2023, 11, 4547–4558

This journal is © The Royal Society of Chemistry 2023

Therefore, continuous ion channels are built finally within the membranes as a result of the obvious difference between the hydrophobic main-chains and the flexible hydrophilic side-chains. The PEMFCs using a Poly(FL50-BP50)-SO$_3$H membrane and ionomer with identical chemical structures deliver comparable power outputs (1.108 W cm^{-2} for H$_2$/air and 2.465 W cm^{-2} for H$_2$/O$_2$) to state-of-the-art aromatic polymer based PEMFCs, and excellent MEA stability greater than 400 h at 0.5 A cm^{-2}. All these results demonstrate that Poly(FLx-BPy)-SO$_3$H PEMs are sufficiently promising candidates for PEMFCs.

Conflicts of interest

The authors declare no conflict of interest.

Acknowledgements

References

1 D. W. Shin, M. D. Guiver and Y. M. Lee, *Chem. Rev.*, 2017, **117**, 4759–4805.

2 W. Li, J. Jiang, H. An, S. Dong, Z. Yue, H. Qian and H. Yang, *ACS Appl. Energy Mater.*, 2021, **4**, 2732–2740.

3 Q. He, T. Xu, H. Qian, J. Zheng, C. Shi, Y. Li and S. Zhang, *J. Power Sources*, 2015, **278**, 590–598.

4 L. Lei, X. Zhu, J. Xu, H. Qian, Z. Zou and H. Yang, *J. Power Sources*, 2017, **350**, 41–48.

5 S. Gao, H. Xu, T. Luo, Y. Guo, Z. Li, A. Ouadah, Y. Zhang, Z. Zhang and C. Zhu, *J. Membr. Sci.*, 2017, **536**, 1–10.

6 J. Han, K. Kim, S. Kim, H. Lee, J. Kim, T. Ko, J. Bae, W. J. Choi, Y.-E. Sung and J.-C. Lee, *J. Power Sources*, 2020, **448**, 227427.

7 J. E. Park, J. Kim, J. Han, K. Kim, S. Park, S. Kim, H. S. Park, Y.-H. Cho, J.-C. Lee and Y.-E. Sung, *J. Membr. Sci.*, 2021, **620**, 118871.

8 D. Yuan, Y. Qin, S. Li, S. Du, Y. Xu, Q. Weng, P. Chen, X. Chen and Z. An, *J. Power Sources*, 2021, **484**, 229265.

9 J. Ahn, R. Shimizu and K. Miyatake, *J. Mater. Chem. A*, 2018, **6**, 24625–24632.

10 P. Y. You, S. K. Kamarudin and M. S. Masdar, *Int. J. Hydrogen Energy*, 2019, **44**, 1857–1866.

11 F. Mack, K. Aniol, C. Ellwein, J. Kerres and R. Zeis, *J. Mater. Chem. A*, 2015, **3**, 10864–10874.

12 J. Chen, L. Wang and L. Wang, *ACS Appl. Mater. Interfaces*, 2020, **12**, 41350–41358.

13 Y. Zhang, Y. Pu, P. Yang, H. Yang, S. Xuan, J. Long, Y. Wang and H. Zhang, *J. Mater. Sci.*, 2018, **53**, 14506–14524.

14 D. Yuan, Y. Qin, S. Li, S. Du, Y. Xu, Q. Weng, P. Chen, X. Chen and Z. An, *J. Membr. Sci.*, 2021, **621**, 118932.

15 A. P. Soleymani, L. R. Parent and J. Jankovic, *Adv. Funct. Mater.*, 2022, **32**, 2105188.

16 X. Liu, J. Zhang, C. Zheng, J. Xue, T. Huang, Y. Yin, Y. Qin, K. Jiao, Q. Du and M. D. Guiver, *Energy Environ. Sci.*, 2020, **13**, 297–309.

17 H. Hu, Y. Sui, M. Ueda, J. Qian, L. Wang and X. Zhang, *J. Membr. Sci.*, 2018, **564**, 342–351.

18 K. Kang and D. Kim, *J. Membr. Sci.*, 2019, **578**, 103–110.

19 B. B. Munavalli and M. Y. Kariduraganavar, *J. Membr. Sci.*, 2018, **566**, 383–395.

20 Z. Yao, Z. Zhang, M. Hu, J. Hou, L. Wu and T. Xu, *J. Membr. Sci.*, 2018, **547**, 43–50.

21 J. Zheng, W. Bi, X. Dong, J. Zhu, H. Mao, S. Li and S. Zhang, *J. Membr. Sci.*, 2016, **517**, 47–56.

22 S. Chandra Sutradhar, M. M. Rahman, F. Ahmed, T. Ryu, l. Jin, S. Yoon, S. Lee, Y. Jin and W. Kim, *J. Power Sources*, 2019, **442**, 227233.

23 M. K. Pagels, S. Adhikari, R. C. Walgama, A. Singh, J. Han, D. Shin and C. Bae, *ACS Macro Lett.*, 2020, **9**, 1489–1493.

24 H. A. Patel, J. Selberg, D. Salah, H. Chen, Y. Liao, S. K. Mohan Nalluri, O. K. Farha, R. Q. Snurr, M. Rolandi and J. F. Stoddart, *ACS Appl. Mater. Interfaces*, 2018, **10**, 25303–25310.

25 M. R. Hibbs, C. H. Fujimoto and C. J. Cornelius, *Macromolecules*, 2009, **42**, 8316–8321.

26 M. S. Cha, J. E. Park, S. Kim, S.-H. Han, S.-H. Shin, S. H. Yang, T.-H. Kim, D. M. Yu, S. So, Y. T. Hong, S. J. Yoon, S-G. Oh, S. Y. Kang, O.-H. Kim, H. S. Park, B. Bae, Y.-E. Sung, Y.-H. Cho and J. Y. Lee, *Energy Environ. Sci.*, 2020, **13**, 3633–3645.

27 N. R. Kang, T. H. Pham and P. Jannasch, *ACS Macro Lett.*, 2019, **8**, 1247–1251.

28 J. S. Olsson, T. H. Pham and P. Jannasch, *Adv. Funct. Mater.*, 2018, **28**, 1702758.

29 P. Zuo, Y. Li, A. Wang, R. Tan, Y. Liu, X. Liang, F. Sheng, G. Tang, L. Ge, L. Wu, Q. Song, N. B. McKeown, Z. Yang and T. Xu, *Angew. Chem., Int. Ed.*, 2020, **59**, 2–12.

30 N. Chen, C. Hu, H. H. Wang, S. P. Kim, H. M. Kim, W. H. Lee, J. Y. Bae, J. H. Park and Y. M. Lee, *Angew. Chem., Int. Ed.*, 2021, **60**, 7710–7718.

31 J. Wang, Y. Zhao, B. P. Setzler, S. Rojas-Carbonell, C. Ben Yehuda, A. Amel, M. Page, L. Wang, K. Hu, L. Shi, S. Gottesfeld, B. Xu and Y. Yan, *Nat. Energy*, 2019, **4**, 392–398.

32 Z. Li, J. Guo, J. Zheng, T. A. Sherazi, S. Li and S. Zhang, *Macromolecules*, 2020, **53**, 10998–11008.

33 N. Chen, H. H. Wang, S. P. Kim, H. M. Kim, W. H. Lee, C. Hu, J. Y. Bae, E. S. Sim, Y. C. Chung, J. H. Jang, S. J. Yoo, Y. Zhuang and Y. M. Lee, *Nat. Commun.*, 2021, **12**, 2367.

34 J. Zhang, K. Zhang, X. Liang, W. Yu, X. Ge, M. A. Shehzad, Z. Ge, Z. Yang, L. Wu and T. Xu, *J. Mater. Chem. A*, 2020, **9**, 327–337.

35 X. Luo, D. I. Kushner, J. Li, E. J. Park, Y. S. Kim and A. Kusoglu, *Adv. Funct. Mater.*, 2021, **31**, 2008778.

36 M. Hwang, K. Nixon, R. Sun, C. Willis and Y. A. Elabd, *J. Membr. Sci.*, 2021, **633**, 119330.

37 X. Pu, Y. Duan, J. Li, C. Ru and C. Zhao, *J. Power Sources*, 2021, **493**, 229671.

38 N. Chen, S. Y. Paek, J. Y. Lee, J. H. Park, S. Y. Lee and Y. M. Lee, *Energy Environ. Sci.*, 2021, **14**, 6338–6348.

39 K. Yang, X. Li, J. Guo, J. Zheng, S. Li, S. Zhang, X. Cao, T. A. Sherazi and X. Liu, *J. Membr. Sci.*, 2020, **596**, 117720.

40 K. Miyatake, H. Zhou, H. Uchida and M. Watanabe, *Chem. Commun.*, 2003, **3**, 368–369.

41 B. Muthuraj, S. Mukherjee, C. Patra and P. Iyer, *ACS Appl. Mater. Interfaces*, 2016, **8**, 32220–32229.

42 Z. Long, J. Miyake and K. Miyatake, *J. Mater. Chem. A*, 2020, **8**, 12134–12140.

43 X. Liu, Y. Li, J. Xue, W. Zhu, J. Zhang, Y. Yin, Y. Qin, K. Jiao, Q. Du, B. Cheng, X. Zhuang, J. Li and M. D. Guiver, *Nat. Commun.*, 2019, **10**, 842.

44 U. Reimer, W. Lehnert, Y. Holade and B. Kokoh, in *Fuel Cells and Hydrogen*, ed. V. Hacker and S. Mitsushima, Elsevier 2018, ch. 2.

45 M. Zago, A. Baricci, A. Bisello, T. Jahnke, H. Yu, R. Maric, P. Zelenay and A. Casalegno, *J. Power Sources*, 2020, **455**, 227990.

4558 | *J. Mater. Chem. A*, 2023, **11**, 4547–4558

This journal is © The Royal Society of Chemistry 2023